Inorganic Chemistry
Article
Cite This: Inorg. Chem. 2018, 57, 12038−12049
pubs.acs.org/IC

Influence of Structural (Cation and Anion) Order in the Superconducting Properties of Ozone-Oxidized $Mo_{0.3}Cu_{0.7}Sr_2RECu_2O_y$ (RE = Yb, Tm, Gd, Nd, and Pr)

Xabier Martínez de Irujo-Labalde, Esteban Urones-Garrote, Susana García-Martín, and Miguel Ángel Alario-Franco*

Departamento de Química Inorgánica I, Facultad de Ciencias Químicas, Universidad Complutense, 28040 Madrid, Spain

Supporting Information

ABSTRACT: The influence of rare earth (RE) elements on superconducting properties of the transition element (TE)-substituted $TE_xCu_{1-x}Sr_2RECu_2O_y$ cuprates has not been sufficiently emphasized so far. In the case of molibdocuprates with the general formula $Mo_{0.3}Cu_{0.3}Sr_2RECu_2O_y$, all the RE element containing compounds except La, Ce, and Lu can be prepared at room pressure. The influence of the crystal structure on the superconducting properties after ozone oxidation of the present system is reported selecting three groups of RE elements attending to their different atom sizes: small (Yb and Tm), medium (Gd), and big (Nd and Pr). Advanced transmission electron microscopy, various diffraction techniques, and spectroscopic analysis have been used to demonstrate that the increase of structural disorder complemented with a decrease in the hole content play a major role in the vanishing of superconductivity within the present system.

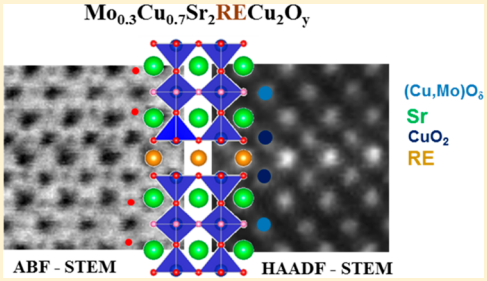

1. INTRODUCTION

Since the discovery of high-temperature superconductivity in oxides of the $La_{2-x}Ba_xCuO_{4-\delta}$ family by Bednorz and Muller in 1986,[1] reporting a critical temperature (T_C) of ∼30 K, attempts to increase the T_C in cuprates rapidly attracted the focus of the field. The appearance of $YBa_2Cu_3O_{7-\delta}$ in 1987,[2] which boosted the T_C above the nitrogen boiling point (77 K) was, indeed, a milestone in this area. In the search for new superconducting materials based on Cu, substitution of Ba by Sr was further proposed, but due to ionic size restrictions, $YSr_2Cu_3O_{7-\delta}$ could only be prepared using high-pressure conditions.[3] However, partial or total substitution of the Cu atoms placed on the charge reservoir layer of the crystal structure by other transition elements (TE) such as Ti, V, Cr, Fe, Co, Nb, Mo, W, Rh, Re, or Ir allowed the formation of phases with the general formula $TE_xCu_{1-x}Sr_2RECu_2O_y$ at ambient pressure.[4−6]

These TE can adopt different oxidation states through oxidizing/reducing reactions resulting in a wider hole doping range than that of the pristine Cu-based superconducting compounds. Indeed, higher valence states for the TE could lead to a greater creation of holes within the charge reservoir layer, which, through a charge transfer process are transferred to the CuO_2 planes. Among TE, Mo stands as an adequate candidate in this type of systems due to its ability to adopt a large number of different formal oxidation states, in particular IV, V and VI in oxides. In this context, ozone-oxidation has been proved successful in increasing the formal oxidation state of some TE due to the high reactivity of the ozone molecule. For instance, the stabilization of uncommon Fe^{4+} in a perovskite-like-structure has been achieved by flowing ozone at relatively low temperature during short times,[7,8] and the ozone technique has also been used for the oxidation of $La_2CuO_{4+\delta}$ thin films providing high oxygen contents.[9]

At room pressure, only a partial substitution of Cu by Mo corresponding to $x = 0.3$ can be achieved in $Mo_xCu_{1-x}Sr_2RECu_2O_y$ for all the rare earth (RE) elements except La, Ce and Lu.[10] The electrical behavior of the whole system indicates that only those compounds containing Nd and Pr do not present superconductivity upon an oxidation treatment.[10] However, in the case of RE = Y and Er under particular oxidation conditions, superconductivity can be induced.[11−13] In this way, although $Mo_{0.3}Cu_{0.7}Sr_2RECu_2O_y$ (RE= Y and Er) compounds do not show superconductivity as synthesized in air, a $T_C \approx 32$ K is achieved after oxidation under oxygen flowing at moderate temperatures. Furthermore, T_C increases under a high-pressure-oxygen treatment reaching T_C's ∼ 70−87 K.[14−18] Therefore, oxidation of these compounds after the synthesis is essential to acquire the adequate amounts of Cu (III) within the CuO_2 planes so as to achieve superconducting properties. It is worth pointing out that hole incorporation in oxidation leads to the shortening of the distance between the copper located at the conducting planes and the apical oxygen ($d(Cu-O_{apical})$) as well as the increasing of the buckling angle between the oxygen and

Received: June 8, 2018
Published: September 19, 2018

DOI: 10.1021/acs.inorgchem.8b01594
Inorg. Chem. 2018, 57, 12038−12049

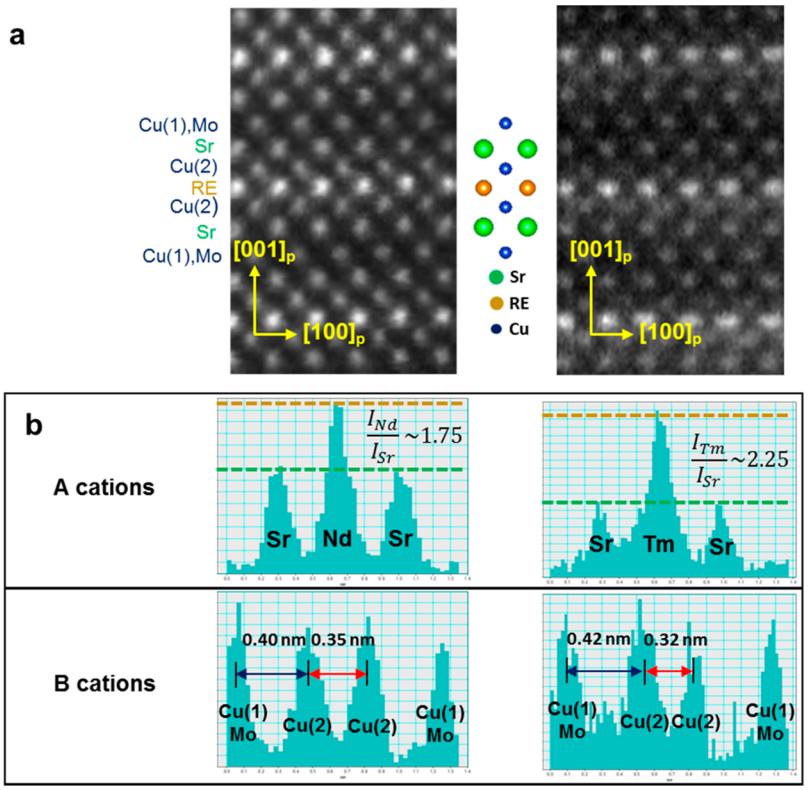

Figure 1. (a) HAADF-STEM images of a $Mo_{0.3}Cu_{0.7}Sr_2RECu_2O_y$ OS crystal with RE = Nd (left) and RE = Tm (right) along the [010]p zone axis. Columns of Sr atoms are indicated in green, RE atoms are in yellow, and columns with either only Cu or both Cu and Mo are in blue. (b) Intensity profiles along the $[001]_p$ direction. The intra- and interbilayer distances in both compounds are indicated with red and blue arrows, respectively.

copper in these planes (θ(O−Cu−O)) which parallels the increase of T_C.[19−21]

In contrast, this shortening of the apical distance is also correlated with other key structural aspect, namely, the relative CuO_2 inter- and intrabilayer spacing, as has been highlighted in pump and probe experiments on the $YBa_2Cu_3O_{7-\delta}$ compound. The femtosecond THz pulses induce a shortening of the apical distance accompanied by a contraction of the so-called interbilayer distance at the expense of the expansion of the so-called intrabilayer resulting in a promoted Josephson coupling.[22,23] Nevertheless, in the case of $Mo_xCu_{1-x}Sr_2RECu_2O_y$ system, the absence of superconductivity in Nd and Pr containing compounds reflects that more subtle structural aspects should be involved.

We report here the influence of the crystal structure on the superconducting properties of the $Mo_{0.3}Cu_{0.7}Sr_2RECu_2O_y$ compounds with RE = Yb, Tm, Gd, Nd, and Pr upon ozone oxidation. We have chosen three groups of RE elements attending to their different size. According to the eight-coordination of the RE cations in this structure, Yb and Tm elements can be considered small (Yb^{3+}: r = 98.5 pm, Tm^{3+}: r = 99.4 pm). Gd is considered medium (Gd3+: r = 105.3 pm), and Nd and Pr are big (Nd^{3+} r = 110.9 pm, Pr^{3+}: r = 112.6 pm).[24]

On the basis of our structural and spectroscopic study of these materials, we demonstrate that the increasing structural disorder and decreasing average oxidation state of Cu, observed when the size of the RE atoms increases, play a crucial role in the vanishing of the superconducting properties in the system. In the case of the nonsuperconducting Nd- and Pr-containing compounds, we have observed antisite disorder between RE and Sr atoms in the crystal structure as well as disorder in the anion sublattice within the charge reservoir blocks. In the case of the Yb and Tm containing compounds, a higher Cu oxidation state is accompanied by a compositional ordering between Sr and RE together with a short-range ordering of oxygen around Cu and Mo, and this allows the materialisation of a superconducting state after the ozone treatment. This is indeed corroborated in that the Gd compound shows an intermediate situation.

2. EXPERIMENTAL SECTION

Polycrystalline compounds, called here original samples (OS), were prepared by the conventional ceramic method using Yb_2O_3 and Tm_2O_3 (Aldrich 99.9%), Gd_2O_3 (Aldrich 99.99%), Nd_2O_3 and Pr_6O_{11} (Aldrich 99.9%), CuO (Aldrich 99.9999%), $SrCO_3$ (Aldrich 99.9%), and Mo powder (Aldrich 99.99%). RE oxides were dried at 1173 K prior to weighing. Stoichiometric amounts of the starting materials were mixed and heated at 1173 K in air to decompose the Sr carbonate. Afterward, the samples containing RE = Tm, Gd, Nd, and Pr were pelletized and heated at 1273 K in air for 48 h with intermediate grindings; the sample containing Yb was heated at 1248 K under the same conditions. All the samples were oxidized using oxygen-containing ozone (ca. 10% vol) at a flow rate of 25 mL min^{-1} for 24 h at 573 K: these are called ozone oxidized samples (OOS).

Phase identification was carried out by powder X-ray diffraction (PXRD) using the PANalytical X'PERT PRO MPD diffractometer with the Cu Kα_1 radiation and X'PERT PEAPS software. To identify the structure and study the arrangement within the unit cell, electron microscopy analyze was performed. The compounds were ground in *n*-butyl alcohol and ultrasonically dispersed. A few drops of the resulting suspension were deposited on a carbon-coated grid. Transmission electron microscopy (TEM) and selectedarea electron diffraction (SAED) studies were performed in a JEOL JEM 3000F microscope operating at 300 kV (double tilt ±20° and point resolution 0.17 nm). High-angle annular dark field (HAADF) and

DOI: 10.1021/acs.inorgchem.8b01594
Inorg. Chem. 2018, 57, 12038−12049

annular bright field (ABF) analyses were performed on an ARM200cF microscope, fitted with a condensed lens aberration corrector (point resolution in STEM mode of 0.08 nm). HAADF images were acquired with an inner acceptance angle of 90 mrad, and the ABF ones have a collection angle of 11 mrad.

The structure determination has been performed by the combination of synchrotron X-ray diffraction in the BM25A Spanish CRG and neutron diffraction at the ESRF neutron diffraction (ND) in the D2B instrument at the ILL. For the Rietveld Refinement the FULLProf software was used.[25] To confirm the oxygen content, thermogravimetric analysis (TGA) has been performed. Samples were heated to 973 K under reducing conditions (5% H_2/95% N_2) obtaining RE_2O_3, SrO, $SrMoO_4$, and Cu metal as final products.

To analyze the Cu oxidation state and the presence of holes in the CuO_2 planes, EELS spectroscopy at Cu−$L_{3,2}$ and O−K edges was performed using an ENFINA spectrometer fitted in the JEOL JEM 3000F microscope. The spectra were collected in the diffraction mode with a dispersion of 0.1 eV/channel for the crystals oriented out of any main zone axis.

Magnetic properties were measured with a Quantum Design MPMS-XL SQUID spectrometer. Temperature dependence of the direct current (dc) magnetic susceptibility under various magnetic fields was measured over the temperature range 2−300 K under zero field cooling (ZFC) and field cooling (FC) conditions. The dc electrical resistance of the samples was measured in a four-probe configuration with a quantum Design PPMS

3. RESULTS AND DISCUSSION

3.1. Structure, Microscopy, and Diffraction. The PXRD patterns of all the compounds except the one containing Yb are characteristic of a single phase with a 3-fold superstructure of the perovskite-type (Figure SI1) and unit cell $a_p \times a_p \times 3a_p$ (a_p is the lattice parameter of the perovskite-type structure). In the pattern of the Yb compound, a small amount of $Yb_2Cu_2O_5$ is detected as a secondary phase.

Electron microscopy analyses have been performed in order to identify the crystal structure of the present system. Figure SI2 shows the SAED patterns along the $[001]_p$, $[100]_p$, and $[1\bar{1}0]_p$ zone axes and the HRTEM image along the $[100]_p$ zone axis of a OS crystal of $Mo_{0.3}Cu_{0.7}Sr_2TmCu_2O_y$. The pattern along the $[001]_p$ zone axis can be indexed on the basis of the cubic perovskite structure. Reflections associated with the tilt of the oxygen-octahedra network do not appear, neither in the $[001]_p$ not along the $[1\bar{1}0]$ zone axes.[26] When tilting the crystal along the $[100]_p$ zone axis, the pattern shows superstructure reflections at $G_p \pm 1/3\ (001)_p$ characteristic of the 3-fold stacking sequence along the $[001]_p$ direction. The corresponding HRTEM image shows contrast differences confirming the triple periodicity along this $[001]_p$ direction. Thus, the combination of the SAED patterns along the different zone axes and the corresponding HRTEM images indicate that the crystal structure of the $Mo_{0.3}Cu_{0.7}Sr_2RECu_2O_y$ system is a perovskite-related superstructure with an $a_p \times a_p \times 3a_p$ tetragonal unit cell according to the arrangement of the Sr and RE atoms in combination with the polyhedral coordination of the Cu atoms (Figure SI3). All the OS compounds of the system show similar SAED and HRTEM results. These results substantiate the proposed crystal structure for all these rare earth compounds (RE= Yb, Tm, Gd, Nd, and Pr).

HAADF-STEM images (Z-contrast images) can give information about the cation arrangement within the structure. Figure 1a shows the corresponding images of the compounds containing Nd and Tm along the $[010]_p$ zone axis before the ozone treatment. The contrast differences in the images confirm the $3a_p$ superstructure along the $[001]_p$ direction associated with the Sr/RE cation ordering for both compounds: the images show an stacking sequence of the A cations layers along the $[001]_p$ direction consisting of two layers with lower-intensity-dots corresponding to columns of Sr cations separated by one layer with higher-intensity-dots corresponding to columns of RE cations. However, the line intensity profiles carried out along the $[001]_p$ direction on the Sr−RE−Sr columns of atoms (Figure 1b) reveal differences in the images of these two compounds. The lower intensity difference between the Sr and RE layers in the Nd compound than that in the Tm one can be associated with some antisite disordering between Nd and Sr. Regarding the B cations, the crystal structure presents two different sites for the Mo and Cu cations: One site is fully occupied by Cu cations constituting the CuO_2 planes, and the other one is occupied by 70% Cu and 30% Mo forming the charge reservoir blocks. Nevertheless, the Z-contrast image do not show intensity differences between these two positions, presumably due to the low amount of Mo within the charge reservoir layers, and its statistical arrangement distribution with the Cu. In contrast, as shown in Figure 1b, a shorter distance between the Cu(2)−Cu(2) columns of atoms, namely, the intrabilayer distance between the CuO_2 planes, is observed in the Tm compound relative to that in the Nd one (0.32 nm for Tm compound and 0.35 nm for Nd compound) at the expense of a larger Cu(2)−Cu/Mo(1) distance (0.42 nm for Tm compound and 0.40 nm for Nd compound as expressed by half of the interbilayer distance).

In order to visualize the anion sublattice in these compounds, ABF-STEM experiments have been carried out. Figure 2 depicts the ABF-STEM image along the $[010]_p$ zone axis of the Nd-OS compound. There are two different types of oxygen environment for the Cu and Cu/Mo atoms: The Cu atoms constituting the CuO_2 planes have a pyramidal anion environment (three columns of oxygen atoms are located around the columns of Cu atoms). However, only two columns of oxygen atoms located along the $[001]_p$ direction are clearly observed around the columns of Cu/Mo atoms, and the intensity of the oxygen columns along the $[100]_p$ direction (indicated in pink color) is so low that a high concentration of anion vacancies are located on those positions along the $[100]_p$ direction. Therefore, a nonoctahedral environment of oxygen is displayed around the Cu and Mo of the charge reservoir layer.

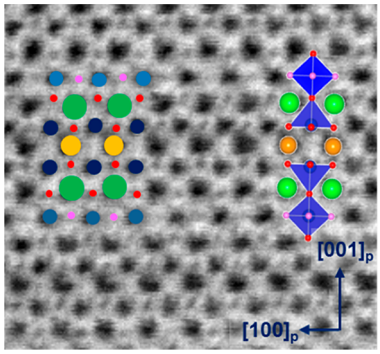

Figure 2. ABF-STEM image of a $Mo_{0.3}Cu_{0.7}Sr_2NdCu_2O_y$ OS crystal along the [010]p zone axis. Columns of oxygen atoms and oxygen/vacancies are indicated in red and pink, respectively. Columns of Sr atoms are indicated in green, columns with Nd atoms are in yellow, columns with only Cu are in dark blue, and columns with both Cu and Mo are in blue.

DOI: 10.1021/acs.inorgchem.8b01594
Inorg. Chem. 2018, 57, 12038−12049

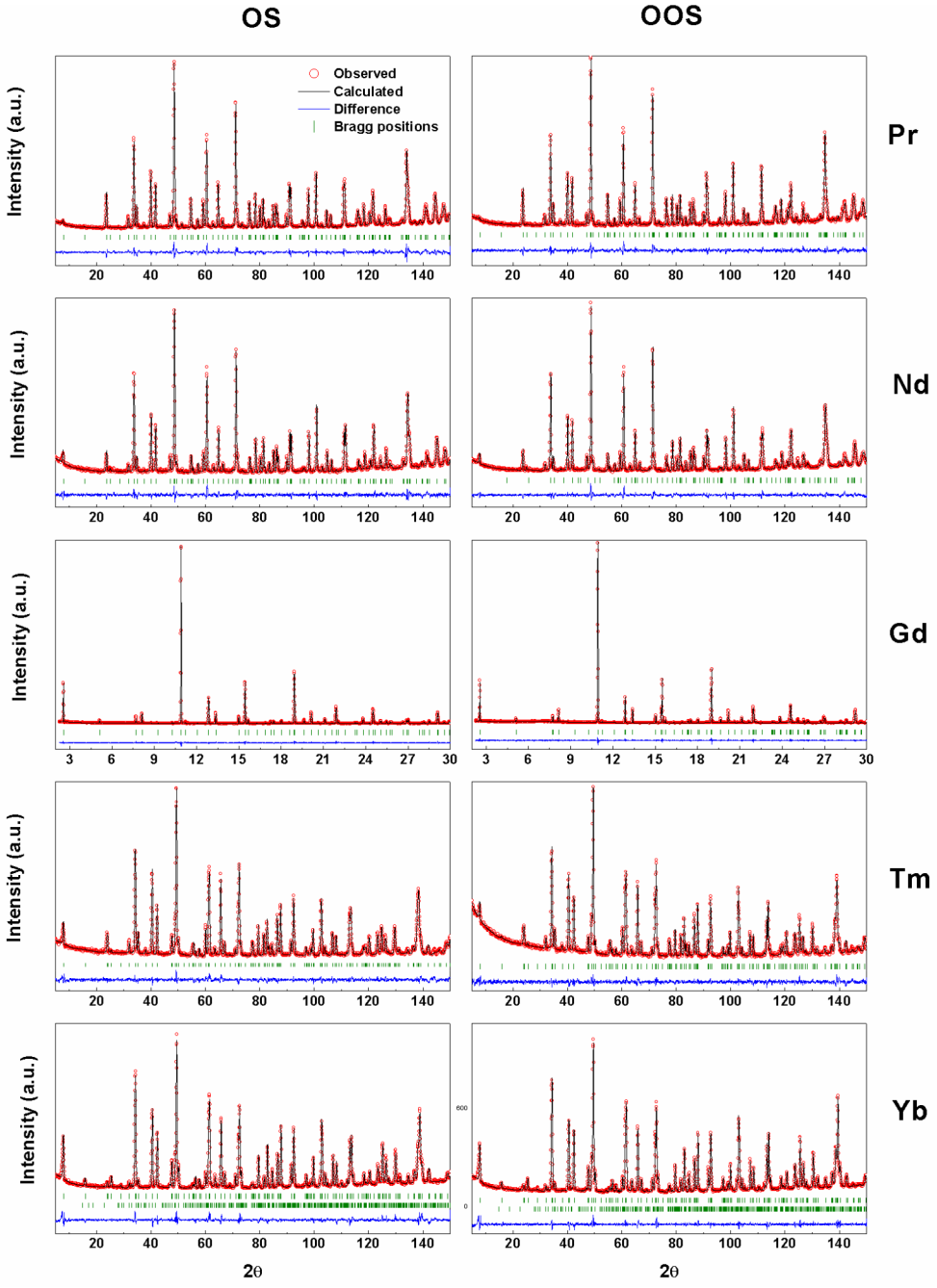

Figure 3. Rietveld refinement of the ND data. Observed, calculated, and difference profiles of the RT patterns of the OS (left) and OOS (right) compounds with formula $Mo_{0.3}Cu_{0.7}Sr_2RECu_2O_y$. 2. 8(2) % of $Yb_2Cu_2O_5$ has been detected as a secondary phase in the diffraction pattern of $Mo_{0.3}Cu_{0.7}Sr_2YbCu_2O_y$.

The presence of Mo in a presumably octahedral coordination and of Cu in a coordination lower than that of Mo, both randomly distributed within the charge reservoir layers (Cu(1) sites in Figure SI3), results in a nonhomogeneous distribution of the oxygen in this area. It is also worth mentioning that the column of apical oxygen atoms of the Cu(1) environment is displaced toward the Mo/Cu atoms, so as to compensate for the anion vacancies within this layer. STEM mapping could not be performed on the OOS compounds due to electron beam damage.

On the basis of these structural results, the synchrotron X-ray and neutron diffraction patterns of all the OS compounds have been indexed using the tetragonal unit cell $a_p \times a_p \times 3a_p$, in space group *P4/mmm*. A joint Rietveld refinement of the SXRD and ND patterns, except for the Gd-one (due to the high neutron absorption of the Gd), has been performed with the main purpose of estimating the occupancies of RE and Sr between the two sites (Figure SI4).Once we obtained the occupancies of the A sites and in order to obtain a more reliable information about the oxygen environments, Rietveld refinement of the ND data of the OS and OOS samples (except the Gd one) has been performed as shown in Figure 3. In the case of the Gd compound, the Rietveld Refinement of SXRD data for the OS and OOS samples have been obtained by fixing the oxygen positions at the average value between those corresponding to the compounds containing Pr and Yb.

DOI: 10.1021/acs.inorgchem.8b01594
Inorg. Chem. 2018, 57, 12038−12049

Table 1. Refined Cell and Atomic Parameters with the Agreement Factors for the Different Compounds OS and OOS[a]

	Pr		Nd		Gd		Tm		Yb	
	OS	OOS	OS	OOS	OS	OOS	OS	OOS	OS	OOS
a (Å)	3.8710(7)	3.8615(0)	3.8661(6)	3.8599(3)	3.8432(9)	3.8308(9)	3.8124(6)	3.8036(4)	3.8069(3)	3.7996(4)
c (Å)	11.638(2)	11.621(8)	11.609(4)	11.595(8)	11.539(6)	11.535(3)	11.537(0)	11.523(2)	11.529(1)	11.515(2)
V (cell volume, Å^3)	174.40(1)	173.29(5)	173.52(8)	172.76(6)	170.45(1)	169.28(9)	167.68(8)	166.71(5)	167.08(9)	166.24(8)
					Mol/Cul [la (0, 0, 0)]					
B_{iso}	2.3(5)	1.5(8)	2.2(2)	1.6(2)	2.5(1)	1.9(1)	1.7(6)	0.9(7)	1.2(3)	0.6(2)
					Cu2 [2g(0, 0, z)]					
z	0.349(7)	0.347(9)	0.350(3)	0.349(7)	0.355(1)	0.352(5)	0.357(7)	0.356(4)	0.358(4)	0.357(1)
B_{iso}	0.0(1)	0.0(1)	0.0(0)	0.0(3)	0.4(1)	0.5(8)	0.2(6)	0.3(7)	0.0(0)	0.0(7)
					REl/Srl [2h (0.5, 0.5, z)]					
z	0.196(6)	0.193(8)	0.196(7)	0.194(8)	0.196(0)	0.192(6)	0.197(2)	0.194(0)	0.197(2)	0.194(5)
occupancy (RE)	0.09(2)	0.09(2)	0.08(8)	0.08(8)	0.03(2)	0.03(2)	−0.0(02)	−0.0(02)	0.0(04)	0.0(04)
B_{iso}	1.2(0)	1.2(6)	1.1(7)	1.1(9)	1.2(8)	1.4(0)	1.3(8)	1.4(6)	1.0(9)	1.0(2)
					RE2/Sr2 [1d (0.5, 0.5, 0.5)]					
occupancy (RE)	0.81(5)	0.81(5)	0.83(0)	0.83(0)	0.93(6)	0.93(6)	1.00(1)	1.00(1)	1.00(2)	1.00(2)
B_{iso}	0.4(2)	0.1(1)	0.1(5)	0.1(1)	0.1(7)	0.3(2)	0.3(5)	0.4(4)	0.3(8)	0.2(0)
					O1 [4n (x, 0.5, 0)]					
x	0.13(1)	0.17(1)	0.14(7)	0.12(5)	0.135	0.120	0.12(2)	0.11(0)	0.12(4)	0.11(6)
occupancy	0.20(1)	0.22(1)	0.21(1)	0.23(1)	0.18	0.22	0.16(1)	0.20(1)	0.16(1)	0.22(1)
B_{iso}	2.2(9)	1.5(8)	2.4(6)	1.6(2)	3.10	2.60	3.5(0)	3.3(1)	3.9(2)	3.6(3)
					O2 [8p (x, y, 0)]					
x	0.70(7)	0.71(4)	0.70(9)	0.72(1)	0.727	0.728	0.73(8)	0.75(2)	0.74(4)	0.74(2)
y	0.41(1)	0.41(6)	0.41(1)	0.40(2)	0.419	0.418	0.43(8)	0.41(7)	0.42(7)	0.42(0)
occupancy	0.080(4)	0.073(6)	0.077(3)	0.074(4)	0.095	0.086	0.096(6)	0.094(4)	0.108(1)	0.098(2)
B_{iso}	2.2(9)	1.5(8)	2.4(6)	1.6(2)	3.10	2.60	3.5(0)	3.3(1)	3.9(2)	3.6(3)
					O3 [4i (0, 0.5, z)]					
z	0.363(7)	0.363(4)	0.364(9)	0.364(7)	0.372(0)	0.369(8)	0.375(3)	0.375(2)	0.375(8)	0.375(5)
B_{iso}	0.4(1)	0.4(3)	0.4(2)	0.4(2)	0.4	0.4	0.7(1)	0.7(3)	0.4(6)	0.5(1)
					O4 [2g (0, 0, z)]					
z	0.157(9)	0.158(2)	0.157(4)	0.158(1)	0.15(9)	0.15(9)	0.159(6)	0.160(2)	0.159(3)	0.159(9)
B_{iso}	2.4(9)	1.9(7)	2.2(9)	2.2(9)	2.0	1.6	1.6(3)	1.4(6)	1.5(1)	1.2(3)
total oxygen content	7.43	7.47	7.44	7.49	7.48 (7.42)	7.56 (7.52)	7.41	7.55	7.51	7.65
R_p	3.75	3.62	3.25	3.06	8.09	8.35	3.84	2.87	3.31	3.33
R_{wp}	4.86	4.60	4.12	3.96	12.2	11.4	4.89	3.58	4.44	4.44
χ^2	5.29	2.34	2.62	2.68	1.32	1.22	2.23	1.99	4.48	4.14

[a]Oxygen positions for the compound containing Gd have been fixed taking into account the corresponding parameters for the compounds containing Pr and Yb. In parentheses are indicated the oxygen contents obtained by the TGA for the OS and OOS compounds.

DOI: 10.1021/acs.inorgchem.8b01594
Inorg. Chem. 2018, 57, 12038−12049

Tables 1 and 2 contain the crystallographic atomic positions, lattice parameters, and main distances and angles of the $Mo_{0.3}Cu_{0.7}Sr_2RECu_2O_y$ compounds obtained from the neutron diffraction data refinements.

Performing the joint refinement in the synchrotron diffraction patterns corresponding to the different compounds, especially to the ones containing bigger RE atoms (Pr and Nd), the intensities of some reflections (i.e., the 001 reflection shown in Figure SI5) cannot be substantiated fixing the Sr and RE in their theoretical positions. The observed decrease of the intensity of the 001 reflection (related to $3a_p$) with increasing the RE size cannot be justified in terms of scattering factors of the corresponding cations fixed in their theoretical sites (Figure SI5). Thus, improved R-factors of the Rietveld refinement are obtained by introducing antisite disorder between Sr and Pr or Nd in the crystal structure, giving a better agreement between the intensity of the experimental and calculated reflections. Moreover, the observed antisite disorder correlates well with the RE size. Figure 4 echoes the variation of the antisite as a function of the RE cation size, showing a mixing between Sr and RE of ∼20% for the Pr and Nd compounds, no mixing for Tm and Yb ones, and an intermediate amount of mixing of ∼6% for the Gd containing one. Therefore, refinement of the crystal structure of $Mo_{0.3}Cu_{0.7}Sr_2RECu_2O_y$ (RE = Pr, Nd) indicates that the antisite disorder suggested in the HAADF-STEM is of a general character and not simply a local arrangement results of the Nd compound. The Rietveld refinement also indicates that the Mo cations are placed within the charge reservoir block for all the compositions.

Complementing the antisite disorder in the A-position, significant differences in the unit cell dimensions are observed for the different RE compounds. The unit cell becomes smaller as the RE size decreases and the c/a ratio decreases from ∼3.03 to ∼3.00 with increasing RE atom size, but this volume change is not isotropic (Figure SI6a). Differences between $c/3$ and a values decrease when the RE atom size increases.

Regarding the oxygen sublattice in the OS samples, the oxygen content varies in the range of 7.40−7.50 (under similar oxidizing conditions) without correlation to the RE size. To establish the oxygen disorder within the charge reservoir layer, we have used a structural model[16] that proposes two different oxygen sites to reflect the variable anion coordination of Mo and Cu: a more symmetrical x-nonfixed to zero oxygen site (x, 0.5, 0) O1 and a less symmetrical x- and y-nonfixed to zero oxygen site (x, y, 0) O2. In this model, it is assumed that the transition metal in an octahedral oxygen environment tends to coordinate with the more symmetrical O1; in contrast, O2 surrounds the lower coordinated cations within the charge reservoir block. Thus, we can expect that the Mo cations are surrounded by O1-type oxygen and that most of the Cu(1) cations are surrounded by O2-type ones. Also, the ratio of oxygen occupancies O1 (x, 0.5, 0)/O2 (x, y, 0) is different for the different compounds. Thus, the refinement gives partial oxygen occupancies of ∼55% for the more symmetrical O1 and ∼45% for the less symmetrical O2 in the Pr and Nd compounds, while the Tm and Yb ones present the opposite ratio (∼45% for O1 and ∼55% for O2). Also, the distribution of the oxygen sites varies between the different compounds (Figure SI7). In the case of Tm and Yb containing compounds, the O2-type oxygen tends to locate closer to O1, implying a certain short-range ordering. However, for the compounds containing Pr and Nd, the O2 atoms spread throughout the

Table 2. Main Distances and Angles for All the OS and OOS Compounds

	Pr		Nd		Gd		Tm		Yb	
distances (Å) and angles (deg)	OS	OOS	OS	OOS	OS	OOS	OS	OOS	OS	OOS
Cu1/Mo1−O1	2.002(15)	1.988(12)	2.01(4)	1.993(15)	1.99046	1.96984	1.962(7)	1.947(3)	1.961(5)	1.950(3)
Cu1/Mo1−O2	1.954(19)	1.949(16)	1.95(2)	1.902(19)	1.92199	1.91049	1.91(3)	1.849(16)	1.895(19)	1.873(19)
Cu1/Mo1−O2	2.547(19)	2.511(16)	2.54(2)	2.545(19)	2.46717	2.46105	2.40(2)	2.406(16)	2.38(19)	2.412(19)
Cu2−O3	1.9423(2)	1.9392(3)	1.9405(3)	1.9379(3)	1.9319(13)	1.9258(12)	1.9170(3)	1.9142(3)	1.9139(3)	1.9116(3)
Cu1/Mo1−O4	1.838(4)	1.839(4)	1.827(3)	1.837(4)	1.832(18)	1.835(19)	1.841(3)	1.846(3)	1.837(4)	1.841(4)
Cu2−O4	2.232(4)	2.205(4)	2.239(6)	2.218(4)	2.265(18)	2.23(2)	2.285(3)	2.261(3)	2.296(4)	2.271(3)
RE−O3	2.502(1)	2.500(1)	2.4897(14)	2.4864(12)	2.422(8)	2.434(7)	2.3883(10)	2.3841(9)	2.3821(10)	2.3798(10)
Sr−O3	2.7440(18)	2.7591(19)	2.748(3)	2.759(2)	2.799(9)	2.801(8)	2.8026(18)	2.8243(18)	2.804(2)	2.820(2)
Sr−O4	2.7740(7)	2.7617(6)	2.7714(9)	2.7618(7)	2.751(3)	2.736(3)	2.7305(5)	2.7177(5)	2.7270(7)	2.7162(6)
RE−Sr	3.532(2)	3.558(2)	3.523(3)	3.539(2)	3.508(3)	3.546(3)	3.493(4)	3.5258(19)	3.492(3)	3.518(3)
d_{intra}	3.498(3)	3.535(2)	3.476(3)	3.486(3)	3.344(7)	3.403(7)	3.284(3)	3.310(3)	3.264(3)	3.290(3)
$d_{inter}/2$	4.0701(14)	4.0432(16)	4.067(2)	4.0551(18)	4.098(5)	4.066(5)	4.1263(16)	4.1067(14)	4.1325(18)	4.1124(18)
O3−Cu2−O3	170.4(3)	169.3(2)	170.0(3)	169.6(3)	168.2(5)	168.1(5)	167.8(2)	166.9(7)	168.0(3)	167.3(3)

DOI: 10.1021/acs.inorgchem.8b01594
Inorg. Chem. 2018, 57, 12038−12049

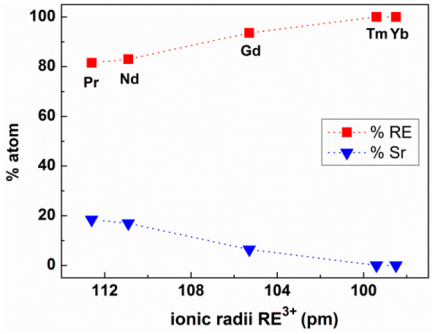

Figure 4. Occupation of RE (red) and Sr (blue) within the (0.5 0.5 0.5) crystallographic position as a function of the RE size.

basal plane of the charge reservoir block, reflecting a great disorder of the Cu oxygen environments. Therefore, the relative occupation and arrangement of the O1 and O2 are displaying structural differences within the charge reservoir blocks between the compounds containing big and small RE elements.

Upon ozone oxidation, all the compounds show a contraction in the cell parameters (Figure SI6b) and larger oxygen occupancy in the O1+O2 sites according to the Rietveld refinement of the neutron data, illustrating its insertion in the charge reservoir layer. An increment in δ of 0.03, 0.10, and 0.16 have been obtained from the TGA confirming the insertion of oxygen with the ozone oxidation. Interestingly, the insertion of oxygen is substantially higher for the compounds containing the smaller RE, reversing the relative O1/O2 oxygen occupancies to obtain ~52 and 48% for Tm and Yb compounds. It is worth mentioning that the distribution of the O1 and O2 remains nearly constant with respect to the OS samples.

Despite the oxygen insertion, no changes in the symmetry of the unit cell are detected for any of the present compounds after oxidation, yet it produces modifications within the crystal structure, which seem to favor the hole transfer from the charge reservoir blocks to the superconducting planes.[27] Thus, the copper–apical oxygen distance decreases upon oxidation, being shorter for the compounds containing bigger RE atoms (Figure 5a). The shortest copper–apical oxygen distance corresponds to the compound containing Pr that should then be expected to have the largest hole concentration in the CuO_2 planes presumably due to the enhancement of the charge transfer. Besides, when the compounds are oxidized, the interbilayer distance decreases at the expense of the intrabilayer distance (Figures 5b,c). The shortening of this distance reduces the size of the insulating block and strengthens the interbilayer coupling via the Josephson effect.[22,23] Again, the shortest interbilayer distance corresponds to the compound containing Pr. Taking into account the variation of these bonding distances (d(Cu–O_{apical})) with the oxidation, it would be expected according to previous works[17,19] that these compounds containing bigger RE atoms will be superconducting and had higher T_C; however, they do not show superconductivity, as shown below

3.2. Transport Properties: Magnetic and Electric Study. Figure 6 shows the temperature dependence of the magnetic susceptibility under 20 Oe for the OS and OOS oxides. None of the OS oxides are superconducting above 2 K. Curie–Weiss fitting of the FC curve at 1000 Oe as a function of temperature (see Figure SI8) in the paramagnetic regime gives effective magnetic moments higher than the theoretical magnetic moment for the corresponding RE for all compounds once the temperature-independent susceptibility of the Cu ions is subtracted (Table 3). This suggests the presence of Mo^{5+}. The negative value of the Curie–Weiss temperature θ for all compounds indicates the antiferromagnetic behavior of the spin interactions. Reversible ZFC-FC curves at 20 Oe are obtained for compounds containing Pr, Nd, and Gd. For the Tm compound, a sharp rise occurs at ~20 K in the ZFC-FC curves that has been associated with a spin glass behavior.[28] In the case of the compound containing Yb, as shown in the inset of Figure 6b, a small bump starts at ~8 K which can be related to the second AF transition of the secondary phase $YbCu_2O_5$.[29] However, the first AF transition at ~15 K characteristic of $YbCu_2O_5$ is not observed. This suggests that the magnetic anomaly detected comes from the presence of Mo^{5+} better aligned on the FC mode in the $Mo_{0.3}Cu_{0.7}Sr_2YbCu_2O_y$ as in the case of $Mo_{0.3}Cu_{0.7}Sr_2YCu_2O_y$.[13]

In Figure 6, we have observed that after the ozone treatment those compounds with bigger RE atoms (Pr and Nd) do not show superconductivity. However, their transport properties change upon the oxidation as shown in the resistivity measurements as a function of temperature depicted in Figure 7. The OS compounds present insulator behavior within the entire temperature regime, while the OOS ones undergo a metal to insulator transition below 170 K. The compound containing Gd presents a sharp decrease of the resistivity below

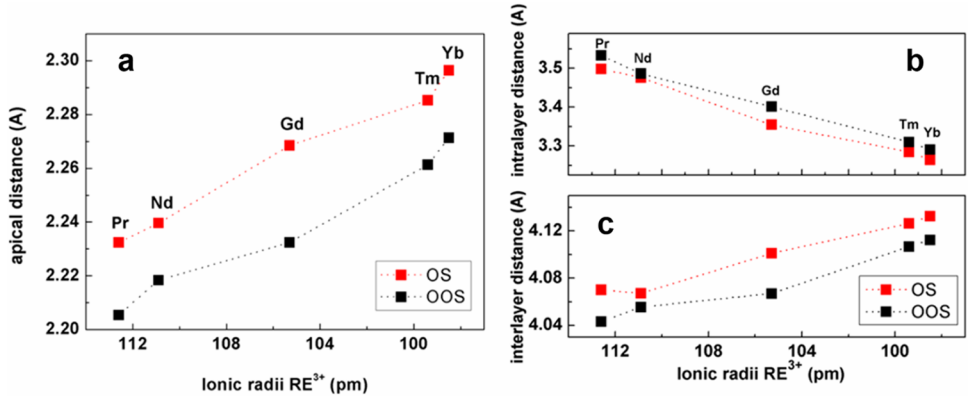

Figure 5. Main RE–O distances as a function of the RE size in the $Mo_{0.3}Cu_{0.7}Sr_2RECu_2O_y$ (RE = Yb, Tm, Gd, Nd, and Pr) compounds: (a) apical, (b) intrabilayer, and (c) interbilayer distances. OS compounds, red; OOS compounds, black.

DOI: 10.1021/acs.inorgchem.8b01594
Inorg. Chem. 2018, 57, 12038–12049

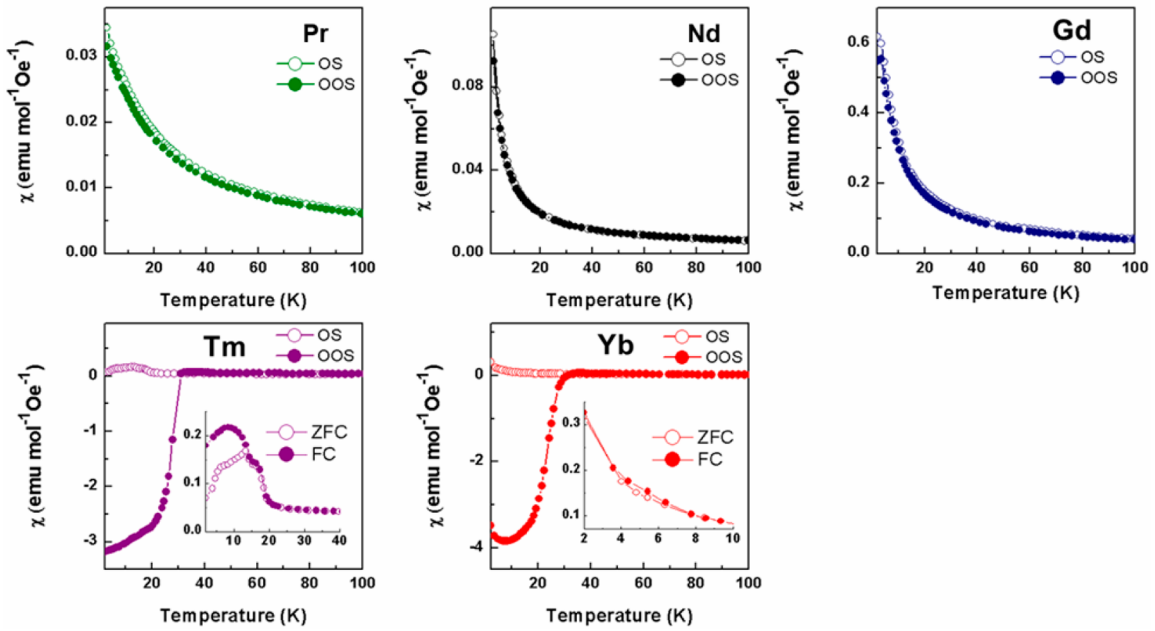

Figure 6. ZFC curves as a function of temperature under a magnetic field H = 20 Oe for the OS and OOS compounds. In the inset, ZFC-FC are depicted for the Tm and Yb OS compounds.

Table 3. Curie Temperature (Θ) and Constant (C) and Magnetic Moment Extracted from the Linear Fitting of the Inverse dc Susceptibility versus Temperature for All the OS Compounds[a]

	Θ (K)	C (emu K mol^{-1} Oe^{-1})	μ_{exp} (μB)	μ_{RE} (μB)
Pr	−43.63	1.69	3.67	3.58
Nd	−50.55	1.77	3.76	3.62
Gd	−3.29	8.06	8.03	7.94
Tm	−35.60	7.02	7.70	7.57
Yb	−110.54	2.85	4.78	4.53

[a]Theoretical magnetic moments of the rare earths have been included to compare with estimated calculated moment.

17 K. Note that the superconductivity in this compound can only be observed in the resistivity behavior and not in the magnetic susceptibility measurements due to the high magnetic moment of the Gd that screens the diamagnetic state for higher magnetic fields than 20 Oe.[30] Finally, for the Tm and Yb compounds, the superconducting transition below ∼32 K can be visualized in both magnetic susceptibility and electrical resistivity. Shielding and Meissner fractions of ∼40−50% and ∼30−40% are obtained below 8 K as shown in Figure 8. The linear dependence of the normalized resistivity with the temperature at the normal state is related to a strange metal behavior localized in the phase diagram of cuprates above optimal doping region.[31]

Therefore, the superconducting behavior of the oxides of this $Mo_{0.3}Cu_{0.7}Sr_2RECu_2O_y$ (RE = Yb, Tm, Gd, Nd, and Pr) system does not follow the expected trend according to the Cu−O_{apical} distances, and only the compounds of lower size (Tm and Yb) are superconducting (with T_C below ∼32 K). Coming back to the crystal structure analysis, we found that the Pr and Nd oxides show the shortest Cu−O_{apical} distances, but they present antisite disordering of the Sr and RE atoms and a more disordered oxygen environment around Cu within the charge reservoir blocks. Structural disorder has been found in other superconducting cuprates, such as those of the $La_{2-x}Sr_xCuO_4$ and $Sr_{2-x}Ba_xCuO_{3+\delta}$ systems, in which the disorder between La^{3+} and Sr^{2+}or betweenSr^{2+} and Ba^{2+} result in depressing of T_C.[32,33] Besides, in the nonsubstituted $Sr_2CuO_{3+\delta}$ compound, the oxygen ordering highly influences the T_C.[21] It seems that the lack of superconductivity is closely related to these structural defects in the $Mo_{0.3}Cu_{0.7}Sr_2RECu_2O_y$ system.

3.3. EELS Spectroscopy and BVS Analysis. The structural disorder in the compounds $Mo_{0.3}Cu_{0.7}Sr_2RECu_2O_y$ (RE= Pr, Nd) does also highly influence the oxidation state of the Cu in the superconducting planes and then the hole-doping level. In order to analyze oxidation state of copper, a BVS study[34] was done using the well-known Zachariasen's equation with b = 0.37 and R_o = 1.600, 1.679, and 1.730 for Cu^{I}, Cu^{II}, and Cu^{III} respectively. Taking into account the distances between oxygen and copper within the structure, the oxidation state of Cu in the planes and reservoir layers and the average oxidation state of Cu within the whole structure have been calculated for the OS and OOS samples as shown in Table 4. First, in the charge reservoir blocks, if we assume the presence of Cu^{II} and Cu^{III}, then the value of BVS obtained is negative. According to previous work,[34] this suggests the presence of Cu^{I} in the materials. The increase of the oxidation state in the charge reservoir layer for the different RE compounds is consistent with the oxygen incorporation after ozone oxidation. However, after oxidation an increase of the amount of Cu^{III} takes place within the superconducting planes. On average, an increase in the Cu oxidation state occurs with the decrease in the RE size. However, this analysis cannot clearly distinguish if the variation in the Mo oxidation state is interfering in the variation of the Cu oxidation state.

Therefore, EELS spectroscopy at the Cu−$L_{2,3}$ edge is an adequate tool to estimate the average Cu oxidation state and to clarify this key problem.[35] The main peak centered at ∼931.2 eV, associated with the transition from Cu 2p $3d^9$ to Cu $\underline{2p}$ $3d^{10}$ (underline denotes the presence of a hole in the Cu 2p orbital), corresponds to the divalent copper Cu^{II}, and the shoulder at ∼932.6 eV, due to the transition from Cu 2p $3d^9\underline{L}$

DOI: 10.1021/acs.inorgchem.8b01594
Inorg. Chem. 2018, 57, 12038−12049

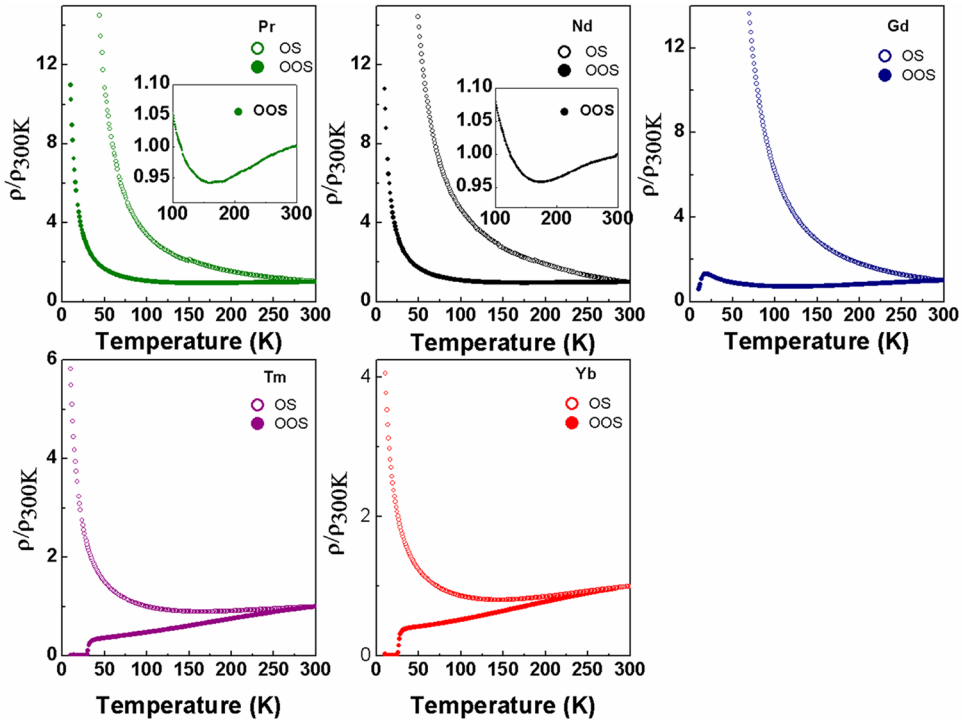

Figure 7. Temperature dependence of the normalized resistivity of the OS and OOS $Mo_{0.3}Cu_{0.7}Sr_2RECu_2O_y$ (RE = Yb, Tm, Gd, Nd, and Pr) compounds. The inset shows metal to insulator transition above 170 K for the Pr- and Nd-containing compounds.

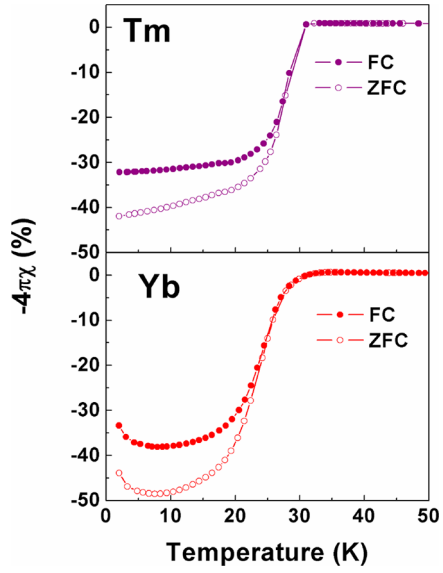

Figure 8. FC-ZFC curves under a magnetic field of H = 20 Oe of the Tm and Yb OOS compounds reflecting the superconducting and Meissner fractions.

to Cu 2p $3d^{10}L$ (underlined L indicates the presence of a hole in the O 2p orbital), is related to trivalent copper Cu^{III} (Figure 9).[35,36] Through the relative intensity of these two peaks fitted with a Voigt function, the average Cu oxidation state has been obtained according to

$$V_{Cu} = 2 + \frac{I_{Cu(III)}}{I_{Cu(III)} + I_{Cu(II)}}$$

The obtained results for the oxidized compounds containing Yb, Tm, Gd, and Nd (Cu–$L_{2,3}$ edge of the compound containing Pr overlaps with the Pr–$M_{5,4}$ edge) confirm the average Cu oxidation state calculated by the BVS analysis. Therefore, the average Cu oxidation state of the oxides with the bigger RE atoms (Pr and Nd) is in agreement with the absence of superconductivity in these compounds.

With regard to the evolution of hole-doping as a function of the RE size, it can be better observed by means of EELS spectroscopy at the O–K edge, which allows identification of the hole transfers to the superconducting planes.[35] In Figure 10a, the broad prepeak at ∼530–531 eV is associated with the transitions in the upper Hubbard band (UHB), while the prepeak at lower energies (∼528.4 eV) is due to the transition from O 1s $3d^9L$ to O 1s $3d^9$ because of the excitation of O 1s electrons to O 1p holes in the superconducting planes.[35,36] In contrast to previous work,[37] in which no change was detected at the prepeak in the O–K edge for the $Y_{1-x}Pr_xBa_2Cu_3O_7$ with Pr introduction, we can observe in Figure 10b a spectral weight transfer to lower energies in parallel with the decrease of the RE size, which indicates a higher hole doping level at the CuO_2 planes for the compounds containing the smallest RE.

Additionally, the O–K edge allows the Sr and RE oxygen environments to be identified in order to confirm the antisite disorder shown from the diffraction techniques. The spectral weight in the region between 532 and 537 eV is associated with the RE–O and Sr–O contributions. In the case of Yb and Tm compounds, two different contributions are clearly observed due to the different sites for Sr and RE. On the contrary, for the Pr and Nd compounds, only one contribution can be observed, indicating similar Sr–O and RE–O distances, which can be attributed to the mixing between Sr and RE in the two sites.

These results show that antisite disordering between the big RE elements (Pr and Nd) and Sr and the lack of ordering of the oxygens around the Cu cations in the charge reservoir blocks affect the hole doping within the CuO_2 planes,

DOI: 10.1021/acs.inorgchem.8b01594
Inorg. Chem. 2018, 57, 12038–12049

Table 4. Cu Oxidation State in the Charge Reservoir Blocks (Cu1) and the CuO_2 Planes (Cu2) and Averaged (Cu_T) Calculated by BVS Analysis for the OS and OOS Oxidized Compounds[a]

	Pr		Nd		Gd		Tm		Yb	
	OS	OOS	OS	OOS	OS	OOS	OS	OOS	OS	OOS
					BVS					
Cu1	1.70	1.76	1.77	1.81	1.76	1.87	1.75	1.94	1.81	1.97
Cu2	2.28	2.33	2.28	2.33	2.33	2.41	2.45	2.49	2.47	2.51
Cu_T	2.13	2.18	2.15	2.19	2.18	2.27	2.27	2.35	2.28	2.38
					EELS					
Cu_T				2.18		2.24		2.38		2.33

[a]For comparison, the average Cu oxidation state determined by EELS spectroscopy for the OOS compounds has been included.

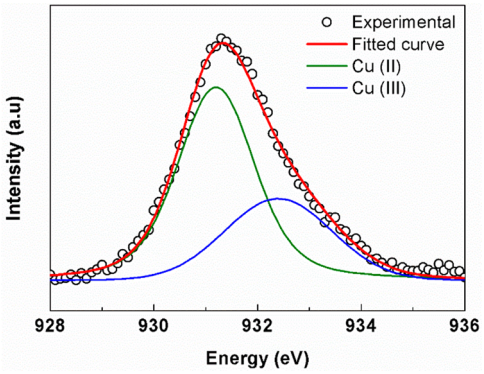

Figure 9. EELS spectra at Cu−$L_{3,2}$ edge for the $Mo_{0.3}Cu_{0.7}Sr_2YbCu_2O_y$ OOS compound. The fitted curve in red results from the sum of the deconvoluted peaks for Cu (II) and Cu (III) in green and blue, respectively.

precluding the superconducting behavior. On the contrary, the Yb and Tm oxides, without antisite disordering and having optimal hole-doping, are superconducting. This point is reaffirmed as the compound containing Gd is located in the under-doped middle region.

4. CONCLUSIONS

We have prepared a series of superconducting oxides in the system $Mo_{0.3}Cu_{0.7}Sr_2RECu_2O_y$, with RE = Tm, Yb, and Gd, by ozone oxidation. The high reactivity of the ozone gas at relatively low temperatures allows one to induce superconductivity in these compounds at ≤32 K with higher superconducting fractions than by other oxidation methods in an optimal doping regime.

The superconducting properties of the $Mo_{0.3}Cu_{0.7}Sr_2RECu_2O_y$ system are very much influenced by the size of the RE, which strongly affects the crystal structure and hole concentration. The molibdo-cuprates of the bigger RE atoms (Pr and Nd) do not show superconductivity despite having the shortest Cu(2)−O_{apical} distances As clearly shown here, these compounds show both RE/Sr antisite disorder and disorder of the oxygen sublattice within the charge reservoir blocks. In order to understand the evolution of the superconducting properties of the cuprates, it is then essential to take into account not only structure and composition but also ordering in both the cationic and anionic sublattices.

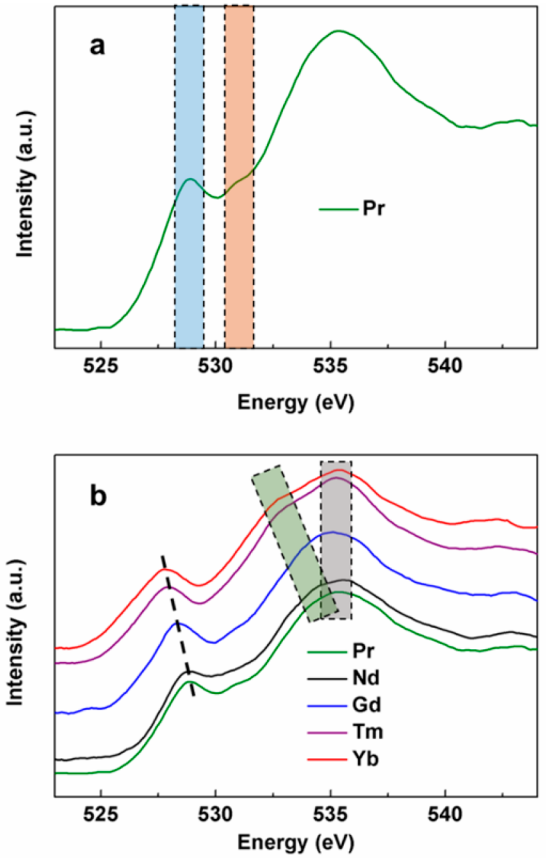

Figure 10. EELS spectra at O−K edge of the $Mo_{0.3}Cu_{0.7}Sr_2RECu_2O_y$ (RE = Yb, Tm, Gd, Nd, and Pr) OOS compounds. In the O−K edge spectra of the $Mo_{0.3}Cu_{0.7}Sr_2PrCu_2O_y$ compound, (a) the two zones in blue and orange corresponding to holes-related peak and UHB peak, respectively, are shown. (b) The O−K edge spectra for all the compounds showing the variation of the hole-related prepeak by a dotted black line are plotted. The marked zones in green and gray correspond to the RE−O and Sr−O signals, respectively.

■ ASSOCIATED CONTENT

Supporting Information

The Supporting Information is available free of charge on the ACS Publications website at DOI: 10.1021/acs.inorgchem.8b01594.

PXRD, SAED, and HRTEM data, crystal structure image, highlight of some selected reflections, plot of the RE size-dependent volume changes, and image of the arrangement of the oxygens within the charge reservoir block (PDF)

DOI: 10.1021/acs.inorgchem.8b01594
Inorg. Chem. 2018, 57, 12038−12049

AUTHOR INFORMATION

Corresponding Author

*E-mail: maaf@quim.ucm.es.

ORCID

Susana García-Martín: 0000-0003-0729-4892

Miguel Ángel Alario-Franco: 0000-0002-6512-7796

Present Address

E.U.-G.: Centro Nacional de Microscopía Electrónica, Universidad Complutense, 28040 Madrid, Spain.

Notes

The authors declare no competing financial interest.

ACKNOWLEDGMENTS

We thank Dr. Romero de Paz for magnetic measurements, Dr. Fernández-Sanjulián for electric measurements, Dr. Ritter for the neutron diffraction measurements, and Dr. Salas-Colera for synchrotron X-ray diffraction measurements. This work has been supported by REE with Project No. REE: 44-2014, Fundación Ramón Areces, by MINECO with Projects MAT2016-78362-C4-4-R and MAT2017-84385-R and CAM with Project MATERYENER3CM-S2013/MIT-2753. X.M.d.I.-L. also thanks MECD for the grant FPU014/05971.

REFERENCES

(1) Bednorz, J. G.; Muller, K. A. Possible high T_C superconductivity in Ba-La-Cu-O system. *Z. Phys. B: Condens. Matter* **1986**, *64*, 189.

(2) Wu, M. K.; Ashburn, J. R.; Torng, C. T.; Hor, P. H.; Meng, R. L.; Gao, L.; Huang, Z. J.; Wang, Y. Q.; Chu, C. W. Superconductivity at 93 K in a new mixed-phase Y-Ba-Cu-O system at ambient pressure. *Phys. Rev. Lett.* **1987**, *58*, 908.

(3) Gilioli, E.; Radaelli, P. G.; Gauzzi, A.; Licci, F.; Marezio, M. Structure and superconductivity of $YSr_2Cu_3O_{7-d}$. *Phys. C* **2000**, *341-348*, 605.

(4) Den, T.; Kobayashi, T. Preparation and properties of $YSr_2Cu_{3-x}M_xO_y$ (M = Li, Al, Ti, V, Cr, Fe, Co, Ga, Ge, Mo, W and Re). *Phys. C* **1992**, *196*, 141.

(5) Greaves, C.; Slater, P. R. The synthesis of new phases related to YBCO by complete replacement of the chain copper sites. *IEEE Trans. Magn.* **1991**, *27* (2), 1174.

(6) Dos Santos García, A. J.; Aguirre, M. H.; Morán, E.; Saez Puche, R.; Alario-Franco, M. Á. A novel ferrimagnetic irido-cuprate: $IrSr_2GdCu_2O_8$. *J. Solid State Chem.* **2006**, *179* (5), 1296.

(7) Hayashi, N.; Yamamoto, T.; Kageyama, H.; Nishi, M.; Watanabe, Y.; Kawakami, T.; Matsushita, Y.; Fujimori, A.; Takano, M. $BaFeO_3$: A Ferromagnetic Iron Oxide. *Angew. Chem., Int. Ed.* **2011**, *50*, 12547.

(8) Hosaka, Y.; Ichikawa, N.; Saito, T.; Manuel, P.; Khalyavin, D.; Attfield, J. P.; Shimakawa, Y. Two-Dimensional Charge Disproportionation of the Unusual High Valence State Fe^{4+} in a Layered Double Perovskite. *J. Am. Chem. Soc.* **2015**, *137* (23), 7468.

(9) Bozovic, I.; Logvenov, G.; Belca, I.; Narimbetov, B.; Sveklo, I. Epitaxial Strain and Superconductivity in $La_{2-x}Sr_xCuO_4$ Thin Films. *Phys. Rev. Lett.* **2002**, *89*, 10170011.

(10) Xiong, Q.; Xue, Y. Y.; Chu, J. W.; Sun, Y. Y.; Wang, Y. Q.; Hor, P. H.; Chu, C. W. High-pressure study of $RSr_2Mo_{0.3}Cu_{2.7}O_y$ with R = Sm, Eu, Gd. Tb, Dy, Ho, Er, Tm, and Yb. *Phys. Rev. B: Condens. Matter Mater. Phys.* **1993**, *47*, 11337.

(11) Hu, S. F.; Liu, R. S.; Su, S. C.; Shy, D. S.; Jefferson, D. A. Crystal Structure and Superconductivity of the Mo-Stabilized Sr-Based $YSr_2Mo_{0.3}Cu_{2.7}O_{7-\delta}$ Compound. *J. Solid State Chem.* **1994**, *112*, 203.

(12) Harlow, R. L.; Kwei, G. H.; Suryanarayanan, R.; Subramanian, M. A. Structure of $YSr_2Cu_{3-x}Mo_xO_{7+\delta}$ (M = Mo, W and Re) from single-crystal X-ray and powder-neutron diffraction. Substituent preference and oxygen defect structure. *Phys. C* **1996**, *257*, 125.

(13) Marik, S.; Moran, E.; Labrugere, C.; Toulemonde, O.; Alario-Franco, M. A. $Mo_{0.3}Cu_{0.7}Sr_2YCu_2O_y$ ($0.3 \leq x \leq 1$) revisited. Superconductivity, magnetism and the molybdenum oxidation state. *J. Solid State Chem.* **2012**, *191*, 40.

(14) Ono, A. High-Pressure Synthesis of Mo-Containing 1212 and 1222 Compounds $(Cu,Mo)Sr_2YCu_2O_z$ and $(Cu,Mo)Sr_2(Y,Ce)Cu_2O_z$. *Jpn. J. Appl. P.* **1993**, *32*, 4517.

(15) Morita, Y.; Nagai, T.; Matsui, Y.; Yamauchi, H.; Karppinen, M. High-T_C superconductivity in three-fluorite-layer copper oxides. II. (Cu, Mo) $Sr_2(Ce, Y)_3Cu_2O_{11+\delta}$. *Phys. Rev. B: Condens. Matter Mater. Phys.* **2004**, *70*, 174515.

(16) Chmaissem, O.; Grigoraviciute, I.; Yamauchi, H.; Karppinen, M.; Marezio, M. Superconductivity and oxygen ordering correlations in the homologous series of $(Cu,Mo)Sr_2(Y,Ce)_sCu_2O_{5+2s+\delta}$. *Phys. Rev. B: Condens. Matter Mater. Phys.* **2010**, *82*, 1045071.

(17) Marik, S.; Labrugere, C.; Toulemonde, O.; Moran, E.; Alario-Franco, M. A. Core-level photoemission spectra of $Mo_{0.3}Cu_{0.7}Sr_2ErCu_2O_y$, a superconducting perovskite derivative. Unconventional structure-property relationships. *Dalton Trans.* **2015**, *44*, 10795.

(18) Gauzzi, A.; Klein, Y.; Nisula, M.; Karppinen, M.; Biswas, P. K.; Saadaoui, H.; Morenzoni, E.; Manuel, P.; Khalyavin, D.; Marezio, M.; Geballe, T. H. Bulk superconductivity at 84 K in the strongly overdoped regime of cuprates. *Phys. Rev. B: Condens. Matter Mater. Phys.* **2016**, *94*, 180509.

(19) Marik, S.; Dos Santos-Garcia, A. J.; Morán, E.; Toulemonde, O.; Alario-Franco, M. A. Oxidation induced superconductivity and Mo/Cu charge equilibrium in $Mo_{0.3}Cu_{0.7}Sr_2ErCu_2O_y$. *Supercond. Sci. Technol.* **2015**, *28*, 0450071.

(20) It is worth mentioning that this shortening of the apical distance is observed within a particular cuprate material; however, the opposite tendency characterizes the different families of cuprates, that is, the longer the apical distance, the higher the T_C. The apical-O distances (d) are d = 2.30 Å for YBCO, 2.43 Å for Bi2212, 2.70 Å for Tl2212, and 2.80 Å for Hg1212, just in the order of increasing T_{Copt}. This is also the order of increasing optical Josephson plasma frequency in the bilayer cuprates.

(21) Uchida, S.-i. *High Temperature Superconductivity: The Road to Higher Critical Temperature*; Springer: London, 2015; p 47.

(22) Hu, W.; Kaiser, S.; Nicoletti, D.; Hunt, C. R.; Gierz, I.; Hoffmann, M. C.; Le Tacon, M.; Loew, T.; Keimer, B.; Cavalleri, A. Optically enhanced coherent transport in $YBa_2Cu_3O_{6.5}$ by ultrafast redistribution of interlayer coupling. *Nat. Mater.* **2014**, *13*, 705.

(23) Mankowsky, R.; Subedi, A.; Först, M.; Mariager, S. O.; Chollet, M.; Lemke, H. T.; Robinson, J. S.; Glownia, J. M.; Minitti, M. P.; Frano, A.; Fechner, M.; Spaldin, N. A.; Loew, T.; Keimer, B.; Georges, A.; Cavalleri, A. Nonlinear lattice dynamics as a basis for enhanced superconductivity in $YBa_2Cu_3O_{6.5}$. *Nature* **2014**, *516*, 71.

(24) Shannon, R. D. Revised Effective Ionic Radii and Systematic Studies of Interatomic Distances in Halides and Chalcogenides. *Acta Crystallogr., Sect. A: Cryst. Phys., Diffr., Theor. Gen. Crystallogr.* **1976**, *32*, 751.

(25) Rodriguez-Carvajal, J. *An Introduction to the Program FULLPROF*; Labratoire Leon Brillouin,CEA-CNRS: Saclay, France, 2001.

(26) Woodward, D. Y.; Reaney, I. M. Electron diffraction of tilted perovskites. *Acta Crystallogr., Sect. B: Struct. Sci.* **2005**, *61*, 387.

(27) Bozin, E. S.; Huq, A.; Shen, B.; Claus, H.; Kwok, W. K.; Tranquada, J. M. Charge-screening role of c-axis atomic displacements in $YBa_2Cu_3O_{6+x}$ and related superconductors. *Phys. Rev. B: Condens. Matter Mater. Phys.* **2016**, *93*, 0545231.

(28) Marik, S.; Dos Santos-Garcia, A. J.; Morán, E.; Toulemonde, O.; Alario-Franco, M. A. Spin glass to superconducting phase transformation by oxidation of a molybdo-cuprate: $Mo_{0.3}Cu_{0.7}Sr_2TmCu_2O_y$. *J. Phys.: Condens. Matter* **2013**, *25*, 165704.

(29) Troc, R.; Klamut, J.; Bukowski, Z.; Horyn, R.; Stepien-Damm, J. On the magnetic ordering in the $R_2Cu_2O_5$. *Phys. B* **1989**, *154*, 189.

(30) Bernhard, C.; Tallon, J. L.; Brücher, E.; Kremer, R. K. Evidence for a bulk Meissner state in the ferromagnetic superconductor

DOI: 10.1021/acs.inorgchem.8b01594
Inorg. Chem. 2018, 57, 12038−12049

$RuSr_2GdCu_2O_8$ from dc magnetization. *Phys. Rev. B: Condens. Matter Mater. Phys.* **2000**, *61* (22), R14960.
(31) Takagi, H.; Batlogg, B.; Kao, H. L.; Kwo, J.; Cava, R. J.; Krajewski, J. J.; Peck, W. F. Systematic evolution of Temperature-Dependent Resistivity in $La_{2-x}Sr_xCuO_4$. *Phys. Rev. Lett.* **1992**, *69*, 2975.
(32) Attfield, J. P.; Kharlanov, A. L.; McAllister, J. A. Cation effects in doped La_2CuO_4 superconductors. *Nature* **1998**, *394*, 157.
(33) Gao, W. B.; Liu, Q. Q.; Yang, L. X.; Yu, Y.; Li, F. Y.; Jin, C. Q.; Uchida, S. Out-of plane effect on the superconductivity of $Sr_{2-x}Ba_xCuO_{3+\delta}$ with T_C up to 98 K. *Phys. Rev. B: Condens. Matter Mater. Phys.* **2009**, *80*, 0945231.
(34) Chmaissem, O.; Eckstein, Y.; Kuper, C. G. Structure and a bond-valence-sum study of the 1−2-3 superconductors (Ca_xLa_{1-x})-$(Ba_{1.75-x}La_{0.25+x})Cu_3O_y$ and $YBa_2Cu_3O_y$. *Phys. Rev. B: Condens. Matter Mater. Phys.* **2001**, *63*, 1745101.
(35) Fink, J.; Nücker, N.; Pellegrin, E.; Romberg, H.; Alexander, M.; Knupfer, M. Electron energy-loss and x-ray absorption spectroscopy of cuprate superconductors and related compounds. *J. Electron Spectrosc. Relat. Phenom.* **1994**, *66*, 395.
(36) Grigoraviciute, I.; Karppinen, M.; Chan, T. S.; Liu, R. S.; Chen, J. M.; Chmaissem, O.; Yamauchi, H. Electronic Structures, Hole-Doping, and Superconductivity of the s = 1, 2, 3, and 4 Members of the (Cu,Mo)-12s2 Homologous Series of Superconductive Copper Oxides. *J. Am. Chem. Soc.* **2010**, *132*, 838.
(37) Fink, J.; Nücker, N.; Romberg, H.; Alexander, M.; Maple, M. B.; Neumeier, J. J.; Allen, J. W. Evidence against hole filling by Pr in $YBa_2Cu_3O_7$. *Phys. Rev. B: Condens. Matter Mater. Phys.* **1990**, *42*, 4823.

DOI: 10.1021/acs.inorgchem.8b01594
Inorg. Chem. 2018, 57, 12038−12049